# Comparative performance analysis of time–frequency distributions for spectroscopic optical coherence tomography

Chenyang Xu, Farzad Kamalabadi, and Stephen A. Boppart

The analysis of spectroscopic optical coherence tomography (SOCT) signals suffers the trade-off between time resolution and frequency resolution. Various joint time–frequency distributions (TFDs) can optimize this trade-off. Synthesized signals were generated and experimentally acquired data were obtained to compare and validate several different TFDs under different SOCT imaging schemes. Specific criteria were designed to quantify the TFD performance. We found that different SOCT imaging schemes require different optimal TFDs. Cohen's class TFDs generate the most compact time–frequency (TF) analysis, while linear TFDs offer the most reliable TF analysis. In both cases, if some prior information is known, model-based TF analysis can improve the performance. 

*OCIS codes:* 170.4500, 110.4500, 300.6500.

## 1. Introduction

In recent years optical coherence tomography (OCT) technology has diverged into specialized applications and techniques.[1–5] One powerful extension to OCT is spectroscopic OCT (SOCT),[6–8] in which not only the intensities but also the spectra of backscattered light are analyzed. Because different tissue structures and molecules have different spectral absorption and scattering properties, spectral analysis, combined with coherence gating, can increase OCT image contrast and generate spatial maps of molecules within samples.[6,9–12] Because the spectra of backscattered light are depth varying along the imaging axis, SOCT signals are typically nonstationary, with both time (depth) and frequency (wavelength) variations. For such nonstationary signals, usual spectral analysis methods, such as the Fourier transform, cannot be used directly because depth-varying information will be lost. Instead, localized spectral analysis methods, or time–frequency (TF) analysis, must be used. The short-time Fourier transform (STFT) and the continuous wavelet transform have been used in SOCT[6,9–11]; however, their performance is complicated by the time–frequency uncertainty principle,[13] which states that there exists an inherent trade-off between spectral resolution and time resolution. Improvement in one implies degradation in the other. Many time–frequency distributions (TFDs) have been studied, each with benefits and drawbacks.[14–17] It is generally accepted that there is no known TFD that is ideal for all cases, but that the best distribution for an application must be chosen based on the properties of the signal and the criteria for the expected result. In this paper our goal is to find the optimal TFDs for different SOCT imaging schemes. It should be noted that in SOCT, "time" directly corresponds to "depth," and "frequency" is usually translated to "wavelength". However, to remain consistent with convention, we use the term "time–frequency" analysis instead of "depth-wavelength" analysis in this paper.

## 2. Models for Spectroscopic Optical Coherence Tomography and Imaging Schemes

OCT measures the interference fringes generated between light beams reflected from a reference mirror and backscattered from scatterers in a sample. For the case of a strong wavelength-dependent scatterer within the coherence length of the optical source and at the axial depth $z$, the interferometric power spec-

C. Xu (cxu@uiuc.edu) and S. A. Boppart (boppart@uiuc.edu) are with the Department of Electrical and Computer Engineering, Beckman Institute for Advanced Science and Technology, University of Illinois at Urbana–Champaign, 405 North Mathews, Urbana, Illinois 61801. F. Kamalabadi is with the Department of Electrical and Computer Engineering, Coordinated Science Laboratory, University of Illinois at Urbana–Champaign, 1308 West Main Street, Urbana, Illinois 61801.

Received 12 July 2004; revised manuscript received 4 October 2004; accepted 20 October 2004.

0003-6935/05/101813-10$15.00/0

trum $I(\lambda, z)$ can be expressed as the product of the source spectrum $S(\lambda)$ and the spectral modification terms, which include the contributions from the spectral backscattering profile $H_r(\lambda, z)$, the lumped spectral modification $H_m(\lambda, z)$ by media along the light path before the scatterer, and the total spectral modification $H_s(\lambda, z)$ by optical components in the system, such as the beam splitter along the optical path. The interferometric power spectrum is given by

$$I(\lambda, z) = S(\lambda)H_r(\lambda, z)H_m(\lambda, z)H_s(\lambda, z). \quad (1)$$

For the cases of multiple scatterers within the coherence length, in general the resulting $I(\lambda, z)$ has spectral modulation owing to the interference of signals from neighboring scatterers. However, this modulation is typically random owing to the random spacing between the scatterers. Therefore, unmodulated spectra from specific areas in the data can still be recovered with high accuracy if sufficient averaging is applied.

In Eq. (1), because $S(\lambda)$ and $H_s(\lambda, z)$ are normally stationary and known *a priori*, measuring $I(\lambda, z)$ offers the opportunity to study the material properties in the sample. SOCT imaging can be divided into two general schemes: imaging the spectral backscattering $H_r(\lambda, z)$ or imaging the media absorption $H_m(\lambda, z)$. These two imaging schemes have different resolution requirements. The spectral backscattering is a short-range effect in that large spectral variations can happen within a very short distance (usually between interfaces such as cell or tissue boundaries). Although high spatial resolution is required, spectral resolution can be somewhat relaxed because large spectral modifications are expected. The spectral absorption and scattering loss, on the other hand, have a relatively long-range effect because they mostly follow the Beer's absorption law. At typical absorber concentrations in tissue, relatively large distances (much larger than the coherence length of the optical source) are usually required to produce significant spectral modification.[9,11] Often with tissue imaging, both effects may coexist. Therefore imaging schemes should be developed that target the dominate effect and reflect the goals of the research.

## 3. Time–Frequency Distributions

Commonly used TFDs fall into one of the following categories: (1) linear TFDs, (2) Cohen's class TFDs, and (3) model-based TFDs. We compare the performance of representative TFDs from each category.

### A. Linear Time-Frequency Domains

Linear TFDs are classical time–frequency analysis methods that involve only linear operations to the time-domain signal. The STFT and Gabor representations are the most familiar examples. The linear TFDs have the advantage in that they are devoid of oscillating cross terms, which are present for many other TFDs. Different TF trade-offs can be made by choosing different time windows. Linear TFDs often lead to good results, but they are compromised by the trade-off between time and frequency resolution owing to a windowing effect. The STFT was included in this study.

### B. Cohen's Class Time–Frequency Domains

The Wigner–Ville distribution (WVD) is the most familiar TFD of the Cohen's class (also called bilinear TFDs). It can achieve better TF resolution than the linear TFDs. The main drawback with the WVD is the presence of strong cross terms if the signal is multicomponent. Cross terms can be suppressed by use of two-dimensional (2-D) low-pass filters (kernels) in the ambiguity domain such as in the smoothed pseudo-WVD (SPWVD). There are many variations of Cohen's class TFDs. One of the best examples is a data-adaptive TFD introduced by Jones and Parks,[16] which employs a radially Gaussian kernel that is signal dependent and that thus changes shape for each signal. The WVD, SPWVD, scalogram with Morlet wavelet, and the Choi–Williams TFDs were implemented in this study.

### C. Model-Based Time–Frequency Domains

In model-based TFDs, the spectrum is not directly calculated. Instead, models and model parameters are estimated and used to reconstruct the spectrum. Models should be carefully chosen based on prior information. For example, if it is known that the dominating spectral modification occurring in a sample is due to the addition of a specific absorbing dye, then a model can be constructed based on the laser spectrum and the dye absorption spectrum to extract the dye concentration distribution in the sample. If no prior knowledge is known, an autoregressive (AR) moving-average (ARMA) model is often used. The time localization of model-based TFDs is achieved by windowing. In this study various models were constructed for different imaging schemes.

Specific expressions for calculating different TFDs are not given in this paper but can be found in the references provided in the introduction.

## 4. Simulated Spectroscopic Optical Coherence Tomography Signals and Time–Frequency Domain Performance Comparison

Because the true TFD of a SOCT signal cannot be known, synthetic signals were generated to produce a comprehensive class of SOCT-like signals controlled by several parameters. Their design was based on Eq. (1) for different imaging schemes. (1) A Gaussian pulse with a spectrum centered at 800 nm and a FWHM of 100 nm. This synthetic signal corresponds to a typical SOCT signal from a perfectly reflecting mirror and is used for testing TFD performance on minimal time–frequency spread. (2) Two consecutive "spectrally absorbed" Gaussian pulses, with the first one containing all of the frequencies of the optical source, and the second one containing only the lower half of the frequencies of the optical source. This sequence corresponds to two closely spaced reflecting interfaces with different spectral reflection profiles.

By varying the distance between the pulses, this sequence was used for testing the minimal spatial separation of TFDs given a prior requirement on frequency resolution. (3) A consecutive Gaussian pulse sequence with random positioning and a slowly varying spectrum between pulses, representing a region of homogeneous absorption and scattering. The absorbers were assumed to uniformly absorb upper-half frequencies, following Beer's law. This sequence corresponds to SOCT signals scattering back from tissue with a roughly uniform scatterer distribution but with high absorber concentrations, and it is used for testing the ability of the TFDs to retrieve the absorption coefficient of the media. To simplify the simulation parameters, we adjusted the sampling time and reference arm translation speed such that the 800-nm laser wavelength corresponded to a digital frequency of 0.125 Hz. The axial depth was converted to a signal acquisition time from 0 to 1 s. Although an experimental OCT system acquires axial scans much faster, these numerically simple parameters can be used without losing theoretical generalities. The synthetic signals and their ideal TFDs are shown in Fig. 1.

For each of the TFDs, parameters are optimized by extensive parameter searching such that they represent the best possible outcome with that type of TFD. In some cases, because good criteria are difficult to obtain, e.g., lowering the cross terms compromises the resolution of the autoterm, qualitative evaluation is used to produce the best analysis.

The TFDs of the signal on the TF plane were generated as color-scale images. In the cases in which the distribution has negative or complex values, the magnitude was taken. A Hamming window was used for the STFT and a Morlet wavelet for the wavelet transform. A Gaussian model was chosen for the model-based TFDs. To compare the overall quality of the TFDs on synthetic signal 1, two criteria are used. The first criterion is the time–frequency spread (by measuring standard deviation) of the TFDs. The second criterion computes the unitless TF concentration or sharpness as follows[16]:

$$C = \frac{\int\int_{\infty} |\mathrm{TFD}(t, f)|^4 dtdf}{\left[\int\int_{\infty} |\mathrm{TFD}(t, f)|^2 dtdf\right]^2}, \tag{2}$$

which is the fourth power of the $L_4$ norm divided by the squared $L_2$ norm of the magnitude of the TFD. The testing results of TFDs on synthetic signal 1 are shown in Table 1. The WVD achieves the best time–frequency concentration. Because the signal model is exactly known for the synthetic signal, the model based TFD completely recovered the ideal TFD.

The ability of TFDs to discriminate two closely spaced yet spectrally different scatterers in SOCT is defined as follows: Two neighboring scatterers are considered to be distinct in SOCT if the maximum shift of the spectral centroid is at least half of what the shift would be if the scatterer were alone. Simple WVD does not perform well under this situation because of the strong cross terms. Instead, the SPWVD was used with a smoothing Gaussian kernel applied independently in the time and frequency directions. Another commonly used TFD, the Choi–Williams distribution, was also investigated. Ideal low- and high-pass filters were used for the model-based TFDs. The minimal distances needed for different TFDs to discriminate the two pulses are listed in Table 2. For reference, the structural OCT resolution (by FWHM criterion) is also listed in Table 2. The Cohen's class TFDs have better performance than the STFT on this synthetic signal.

The third test signal was used for testing the capability of different TFDs to accurately retrieve absorption spectra from a homogeneously absorbing media. The absorption is assumed to follow Beer's Law. The locations of the scatterers were first identified by peak detection. Then absorption spectra were determined from TFDs based on least-square curve fitting of TFDs from multiple scatterers. The error function was calculated from the measured absorption spectra $A'(f)$ and the expected absorption spectra $A(f)$ using the following formula:

$$\mathrm{error} = \sum_{\text{frequency band}} \frac{A'(f) - A(f)}{A(f)}. \tag{3}$$

The frequency band was defined by the 10% level criterion. For the model-based TFD, ideal LPFs were used. The errors for different TFDs are listed in Table 3. The model-based TFD outperforms all other TFDs. Linear TFDs are reasonably good, whereas all Cohen's class TFDs give erroneous outcomes owing to cross terms and nonideal smoothing operations.

### 5. Experimental Spectroscopic Optical Coherence Tomography Signals and Time–Frequency Domain Performance Comparison

Based on simulation data, we observe that in SOCT applications in which physical models of scatterers exist, model-based TFDs can achieve almost ideal TF resolutions. Cohens' class TFDs can generate the most compact TF analysis, and the linear TFDs offer faster and more reliable TF analysis. In this section we evaluate these findings by applying different TFDs on a few specifically designed SOCT imaging experiments in which most, if not all, system and sample parameters are known. The SOCT signal from a highly reflecting mirror surface was nearly the same as the synthetic signal 1 and yielded nearly identical results. Therefore these findings were omitted from the discussions below.

#### A. Spectroscopic Optical Coherence Tomography Experiments for Closely Spaced Interfaces

For synthetic signal 2, the two backscattering interfaces are spatially close and exhibit different back-

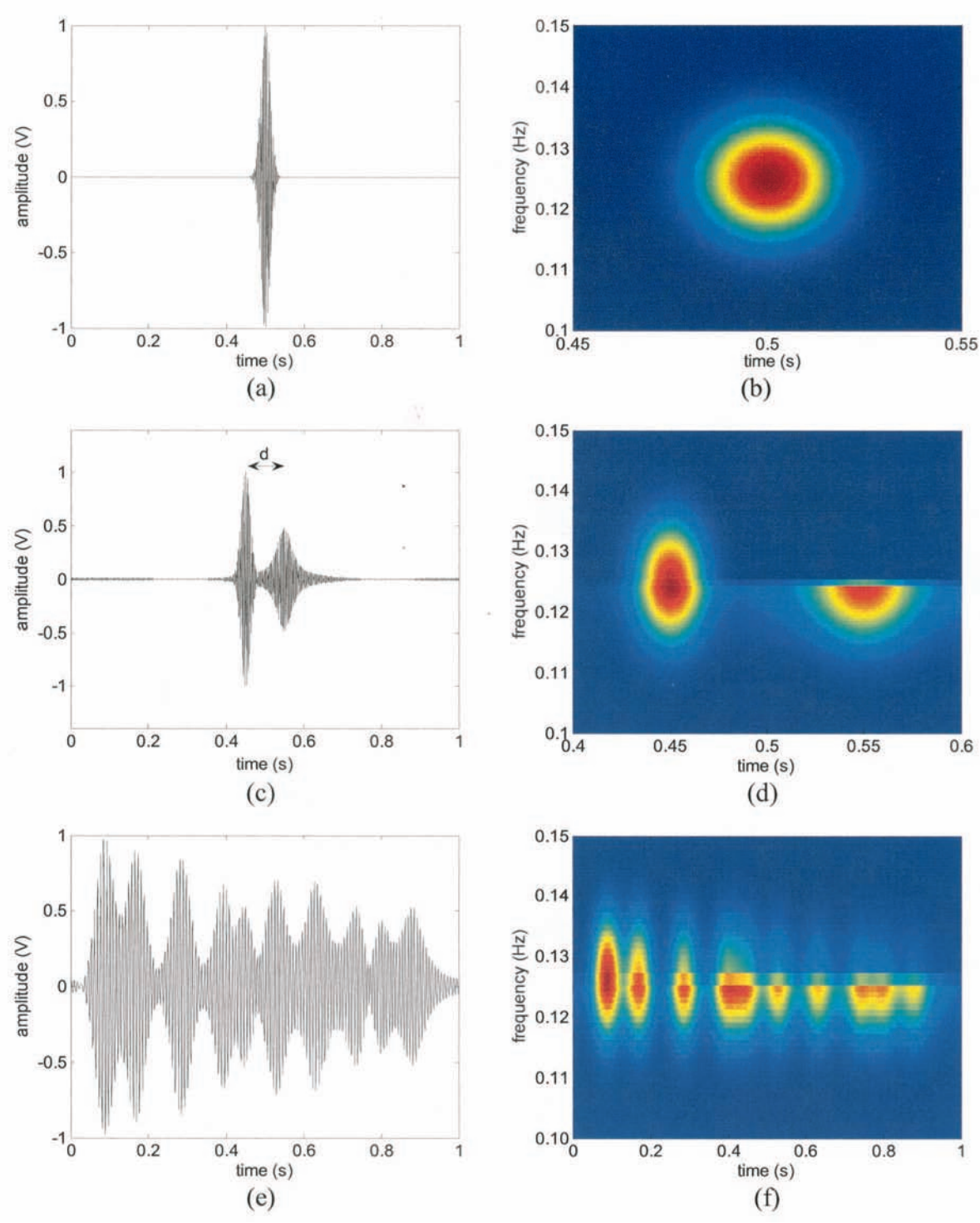


Fig. 1. SOCT synthetic signals: (a) synthetic signal 1, (b) ideal TFD of (a), (c) synthetic signal 2, (d) ideal TFD of (c), (e) synthetic signal 3, (f) ideal TFD of (e).

scattering spectra. To mimic this we constructed an experimental test sample, as shown in Fig. 2. Double-sided tape (~80 μm thick) was placed between and along one edge of two 24 × 60 mm glass coverslips. A paper clip compressed the coverslips at the opposite edge to make a semiclosed thin gap between the two coverslips. The assembly was then turned vertically, and one wedge-shaped open side was submerged into a shallow 20-mg/ml solution of near-infrared (NIR) dye (SDA7460, H. W. Sands Corp.). After a few seconds, the dye solution filled the wedge-shaped space between the coverslips via capillary forces. This particular NIR dye offers many advantages for SOCT.[10] It has very high absorptivity and selectively cuts off

Table 1. Comparison of Time–Frequency Resolution of the TFDs on Synthetic Signal 1

| Parameter | TFD Type | | | | |
|---|---|---|---|---|---|
| | Ideal TFD | STFT | WT | WVD | Model Based |
| Time spread (s) | 0.027 | 0.032 | 0.040 | 0.020 | 0.027 |
| Frequency spread (Hz) | 0.016 | 0.032 | 0.038 | 0.022 | 0.017 |
| Time–frequency product | $4.32 \times 10^{-4}$ | $1.02 \times 10^{-3}$ | $1.52 \times 10^{-3}$ | $4.40 \times 10^{-4}$ | $4.59 \times 10^{-4}$ |
| Concentration | 250 | 102 | 132 | 305 | 250 |

the shorter wavelengths of the laser spectrum used in our OCT system (Fig. 3). Unlike many other water-soluble NIR dyes, this dye strictly follows Beer's law of absorption up to very high concentrations. Even at 20 mg/ml, the dye still maintains its expected absorption spectrum. No photobleaching effect was observed with 10 mW of focused laser power over a period of 10 min.

The sample was imaged with a fiber-based time-domain OCT system with a broadband Ti:$Al_2O_3$ laser source (Kapteyn–Musnane Labs; $\lambda_c = 795$ nm, $\Delta\lambda = 120$ nm, $P_{out} = 10$-mW exit fiber at sample arm). Dispersion and polarization were matched in the interferometer arms. A thin lens with a 40-mm focal length was chosen to minimize the effect of chromatic aberration, dispersion, and focusing. A precision linear optical scanner was used to scan the reference arm. Nonlinearities in the reference scanning rate were accounted for by acquiring a reference fringe pattern with a narrowband laser diode ($\lambda_c = 776$ nm, $\Delta\lambda = 1$ nm) and by applying a data correction algorithm. The OCT system provided a 4-μm axial resolution with a 3.2-mm depth of focus (confocal parameter) in air. The interference was detected by use of an autobalancing detector (Model 2007,

Table 2. Comparison of Minimal Resolving Distance of the TFDs on Synthetic Signal 2

| TFD Type | Minimal Distance (s) |
|---|---|
| Structural OCT | 0.053 |
| Ideal TFD | 0.025 |
| STFT | 0.036 |
| WT | 0.039 |
| SPWVD | 0.033 |
| Model based | 0.026 |

Table 3. Comparison of TFD Performance for Retrieving Absorption Spectra on Synthetic Signal 3

| TFD Type | Error (%) |
|---|---|
| Ideal TFD | 0.0 |
| STFT | −5.0 |
| WT | −6.1 |
| SPWVD | 34.3 |
| Model based | 0.0 |

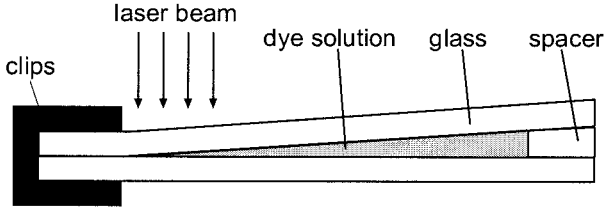


Fig. 2. Sample construction for obtaining SOCT signals from two closely spaced interfaces. The geometrical dimensions are given in the text.

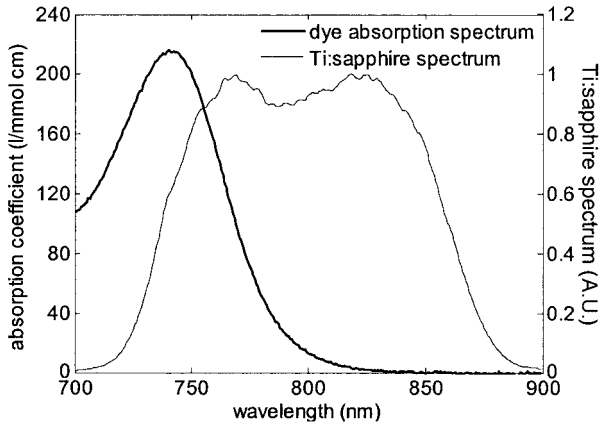


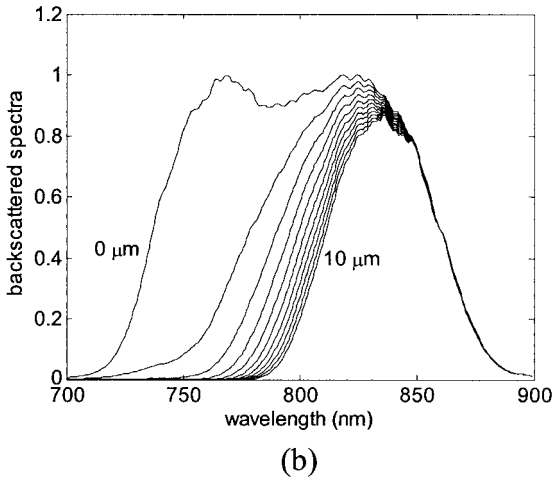


Fig. 3. NIR dye properties. (a) Absorption spectra from NIR dye and emission spectrum of the Ti:sapphire laser used in this study. (b) Theoretical backscattered spectra for dye layer thicknesses from 0 to 10 μm.

New Focus, Inc.). The signal was then amplified and filtered by use of an antialiasing low-pass filter in a custom analog circuit. A high-speed (5-Msamples/s, 12-bit) A/D converter (NI-PCI-6110, National Instruments) was used to acquire the interferometric fringe data. Before application of the TFD analysis, the signal was bandpass filtered to remove excessive noise in the digital domain and was digitally corrected for dispersion.[18]

Axial scans along different wedge positions (different dye thicknesses) were acquired. The sample was placed on an angle-adjustable stage such that the light reflected back from the glass–liquid interface was in a near-normal direction. The incident laser power was attenuated to prevent saturation at the photodetector. The interference fringe data were collected for analysis with different TFDs. The interference fringes resulting from multiple reflections (light bouncing back and forth between the two glass interfaces) were found to have magnitudes at least 50 times smaller than those of the main interference fringes and therefore could be neglected in our analysis.

Figure 4 shows the interferogram signals of two interfaces at various distances and their STFT magnitudes. The windows chosen for the STFT were Hamming windows with a length corresponding to one coherence length of the incident laser. The actual distance between the two interfaces in terms of coherence lengths was measured by counting the number of fringe peaks between two pulse centers and the number of fringe peaks between the FWHM from a single pulse off a mirror. One can observe that most of the shorter wavelengths are absent from the light reflected from the lower dye–glass interface because of the dye absorption. One can also observe the blurring of the time–frequency representation as the separation of the two interfaces narrows, as expected from the uncertainty principle. Specifically, when the distance between the two interfaces was less than the coherence length of the optical source, it became difficult to resolve them. Furthermore, this representation is comparable with the time–frequency representation of a synthetic signal with the full spectrum reflected off the first interface and half of the spectrum reflected off the second interface (data not shown).

It is therefore interesting to test which TFDs will have the greatest TF resolving power in this setting. The STFT, scalogram, Choi–Williams distribution, and model-based TFDs were chosen for comparison. The length of time windowing for the STFT and the Choi–Williams distribution was chosen to correspond to 1 μm in air. This length offers the best separation by qualitative assessment. Morlet wavelets were chosen for the scalogram. The model for the model-based TFD is set up as follows. Assume that the TFD of the pulse from the first interface is the same as the WVD of a pulse from a mirror [$\mathrm{TFD}_M(z, \lambda)$] except for a scaling factor, and that the TFD of the pulse from the second interface is the first TFD after dye absorption multiplied by another scaling factor,

$$\mathrm{TFD} = A \times \mathrm{TFD}_M(z, \lambda) + \mathrm{TFD}_M(z - z_t, \lambda) \times \exp[-B\epsilon(\lambda)], \quad (4)$$

where $A$ and $B$ are the scaling factors and $z_t$ is the distance between the two interfaces. Equation (4) is digitized in $z$ and $\lambda$ to have each $z$ point represent 0.1 μm and each $\lambda$ point represent 1 nm. The term $\epsilon(\lambda)$, representing dye absorptivity, was measured by a spectrometer. Spline interpolations were used whenever the experimentally measured data had data points different from the model. The criterion for model optimization is to search for the best $A$, $B$, and $z_t$ such that the lowest mean-square error between the model TFD and the TFD obtained by STFT is generated. Because it is computationally expensive to search for three optimal parameters $(A, B, z_t)$ in three-dimensional (3-D) space, we first determined $z_t$ based on the fringe number and searched only for the optimal $A$ and $B$ in 2-D space and then determined the optimal $z_t$ for that $A$ and $B$. The two-step recursion was repeated until results stabilized. If fast algorithms are developed, a 3-D direct parametric search without prior knowledge of $z_t$ would be possible.

Figure 5 shows the TFDs for the signal in Fig. 4(e). The TFDs from Cohen's class (the Choi–Williams distribution and scalogram) have comparative performance, and both perform better than the STFT. The artifacts on the top of the TFD plots for the Choi–Williams distribution [Fig. 5(b)] are due to the cross terms during the bilinear transformation of the signal. However, because the cross terms are outside the primary signal bands, they can be rejected easily. As shown in the simulation and confirmed experimentally, the model-based TFD has the best performance in terms of sharpness, although it may or may not be representing the true TFD.

### B. Spectroscopic Optical Coherence Tomography Experiments for Absorbing Regions

In synthetic signal 3, the absorption coefficient was retrieved from of a homogeneous medium containing a small amount of scatterers. To experimentally replicate this, we made phantoms in liquid form for easy handling and accurate concentration control. NIR dye (ADS830WS, American Dye Sources, Inc.) was used. Unlike the dye SDA7460 used in the previous experiment (Subsection 5.A) this dye has a sharp absorption peak around 810 nm, which is close to the emission spectrum of the laser source. Having an absorption peak near the center of the laser source spectrum facilitates the evaluation of the performance of different TFDs. When dissolved in methanol, this dye is also very stable and does not show any photobleaching effect under 10 mW of focused laser power over a period of 10 min. Silica microbeads 0.33 μm in diameter (Bang Laboratories, Inc.) were used as scattering agents. The solution containing the dye and microbeads was placed inside a thin glass cuvette and was imaged with the same SOCT setup used in the previous experiments (Subsection 5.A).

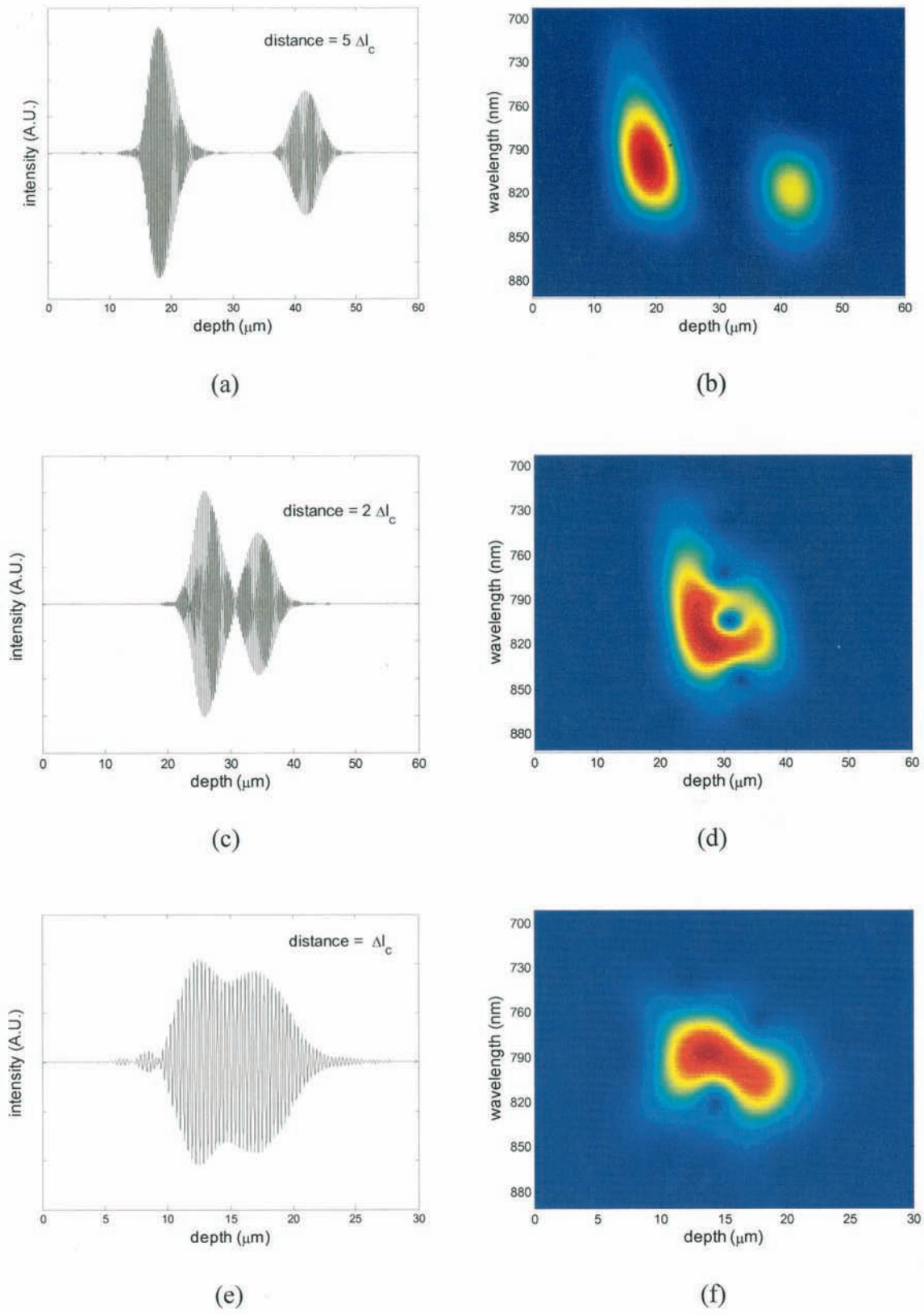


Fig. 4. STFT of SOCT signals backreflected from two glass interfaces separated by various distance with NIR dye in between: (a) SOCT signal for distance = 5 $\Delta l_c$ (coherence lengths), (b) STFT of signal in (a), (c) SOCT signal for distance = $2\Delta l_c$, (d) STFT of signal in (c), (e) SOCT signal for distance = $\Delta l_c$, (f) STFT of signal in (e). Note that the $x$-axis scale is half for (e) and (f) to improve visualization of these two closely spaced pulses.

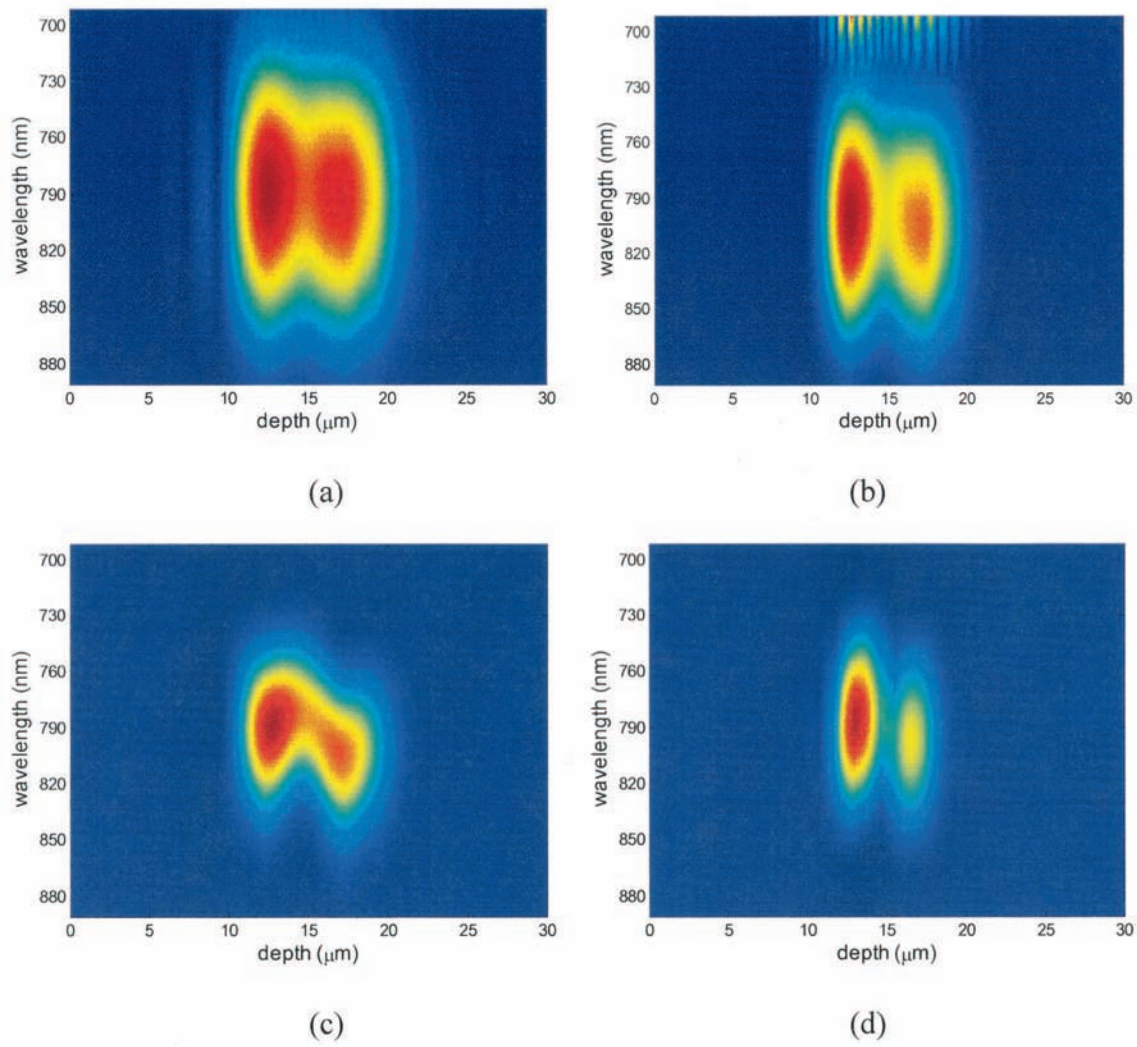


Fig. 5. Different time–frequency representations of the signal in Fig. 4(e). (a) STFT with Hamming window of length corresponding to 1 μm. (b) Scalogram with the Morlet wavelet. The analyzing wavelet of half-length corresponds to 1 μm in air. (c) Choi–Williams distribution with time-smoothing window of length corresponding to 1 μm in air. (d) Model-based TFD as described in the text. Note the cross-term artifacts shown above the main signal in (b).

The concentrations of the dye and silica microbeads were adjusted such that the absorption loss was 5 times larger than the scattering loss at 800 nm. Before SOCT imaging, the mixture was measured by a spectrometer for the combined effect of absorption loss and scattering loss. The absorption spectra were retrieved by each TFD method, similar to the analysis on synthetic signal 3 except for three additional modifications. First, a control sample containing the same concentration of microbeads, but without dye, was used for data correction to reduce the system error. Second, because very closely spaced scatterers exhibit a significant spectral-interference effect, averaging of TFDs from 512 scan lines was performed to obtain the final TFDs. Third, because of the large number of data points collected (50, 000 points/scan line), it was not possible to perform different TFDs directly without significant computational complexity. Therefore, taking advantage of the fact that the SOCT signals are narrow passband signals, data were demodulated and decimated to obtain the shortest possible analytic signals without losing frequency information within the laser source spectrum. The time window sizes for the STFT, Choi–Williams distributions, and the model-based TFDs were chosen to be equivalent to a coherence length of 4. The Morlet wavelet was used for the wavelet transform. Because no prior information was assumed, an AR model with the Burg method was used for the model-based TFDs, with a model order set to 4. The absorption spectra obtained by different TFDs are shown in Fig. 6. For comparison, each spectra was normalized to its respective peak value. From the figure, it is obvious that in this SOCT imaging scheme, the STFT and the wavelet transform are the reliable methods. The model-based TFD has reasonably good performance, even though no assumption was made when the model was constructed. The spectrum retrieved with the Choi–Williams TFD is totally random. These results agree with what our simulations predicted.

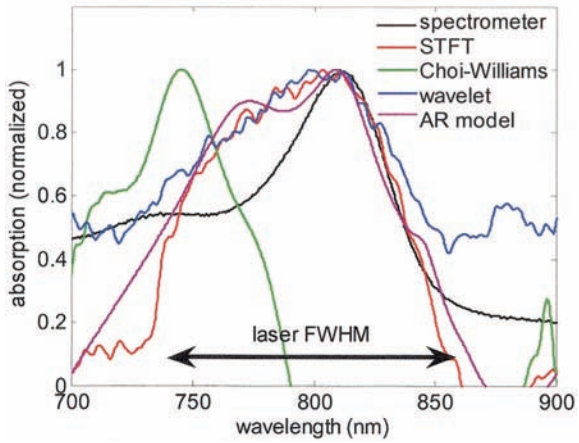


Fig. 6. Comparison of extracted absorption spectra. Curves represent extracted absorption spectra from a dye-filled cuvette with different TFDs, compared with the mixture absorption spectra measured with a spectrometer. The spectral range of the laser (FWHM) is also shown, within which the absorption spectra of the media can be determined.

## 6. Discussion and Conclusion

Ideally, one should be able to find the best TFD that is optimal for resolving minute time–frequency variations. However, various trade-offs between different TFDs and different parameter choices within TFDs, together with the wide application range of SOCT, make it a challenge to find the optimal combinations. The STFT has a simple intuitive interpretation and, by choosing windows of different lengths, one can make different resolution trade-offs. However, one must manipulate the window depending on the quantities being estimated. For example, Figs. 4(f) and 5(a) are both STFTs on the same signal, but because of the difference in window length, one can resolve the spectral variation only in Fig. 4(f) and the time variation only in Fig. 5(a). For two interfaces that are very closely spaced, the STFT often cannot resolve the components effectively. From TFD performance testing results on simulated and experimental data, we see that Cohens' class TFDs can, in most cases, generate the most compact TF analysis compared with the STFT, and therefore they are more appropriate for imaging spectral reflections where higher time–frequency resolution is desired. However, Cohen's class TFDs suffer from the fact that for multicomponent signals, artifacts are generated. Fortunately, this problem can be mitigated by the fact that many kernel-based TFDs have a significantly reduced artifact level and that the SOCT signals are usually narrow passband signals that correspond only to the laser spectrum used in the experiments. Frequently, the artifacts from the TFDs are outside the passband and can therefore easily be removed by filtering.

The increase in joint time–frequency resolution offered by Cohen's class TFDs is not always useful in all SOCT imaging applications. When imaging based on tissue absorption or when using low concentrations of dyes as contrast-enhancing agents, a long path length is frequently necessary to produce a detectable absorption change in the signal. For this case, even the STFT, with its lower spatial resolution, can be sufficient. Because the STFT is totally devoid of artifacts, the STFT is the most reliable for such applications. In addition, computing the STFT is significantly faster than other TFDs because of the use of the fast Fourier transform. The flexibility of digital processing permits essentially arbitrary transformation. One could potentially run a fast and less-accurate STFT first, identify the potential absorbing and spectrally reflecting locations, and then run different TFDs in the desired regions to obtain the best information. In fact, from the figures, one can see that when the scatterers are very close together (comparable with the coherence length), the usual spectral analysis methods are not reliable. One cannot simply assume that the frequency components shown on the TFD plots are actually the frequency components representative of that particular spatial point. Instead, pattern analysis algorithms are better suited for identifying different objects. It is therefore obvious that digital signal processing algorithms applied to experimentally acquired OCT data will become increasingly important for extracting diagnostic and quantitative information.

We thank Daniel Marks and Amy Oldenburg for their technical contributions and for improvements to our OCT systems, and we thank Jing Tang for her technical insight into digital signal processing algorithms. This research was supported in part by grants from the Whitaker Foundation (RG-01-0179; S. A. Boppart), from NASA and the National Cancer Institute (NAS2-02057, S. A. Boppart), and from the National Institutes of Health (1 R01 EB00108-1, S. A. Boppart).

## References

1. D. Huang, E. A. Swanson, C. P. Lin, J. S. Schuman, W. G. Stinson, W. Chang, M. R. Hee, T. Flotte, K. Gregory, C. A. Puliafito, and J. G. Fujimoto, "Optical coherence tomography," Science **254,** 1178–1181 (1991).
2. J. G. Fujimoto, M. E. Brezinski, G. J. Tearney, S. A. Boppart, B. E. Bouma, M. R. Hee, J. F. Southern, and E. A. Swanson, "Biomedical imaging and optical biopsy using optical coherence tomography," Nat. Med. **1,** 970–972 (1995).
3. J. F. de Boer, T. E. Milner, M. J. C. van Germert, and J. S. Nelson, "Two-dimensional birefringence imaging in biological tissue by polarization sensitive optical coherence tomography," Opt. Lett. **22,** 934–936 (1997).
4. S. A. Boppart, B. E. Bouma, C. Pitris, F. F. Southern, M. E. Brezinski, and J. G. Fujimoto, "*In vivo* cellular optical coherence tomography imaging," Nat. Med. **4,** 861–864 (1998).
5. S. A. Boppart, B. E. Bouma, C. Pitris, G. J. Tearney, J. F. Southern, M. E. Brezinski, and J. G. Fujimoto, "Intraoperative assessment of microsurgery with three dimensional optical coherence tomography," Radiology **208,** 81–86 (1998).
6. U. Morgner, W. Drexler, F. C. Kartner, X. D. Li, C. Pitris, E. P. Ippen, and J. G. Fujimoto, "Spectroscopic optical coherence tomography," Opt. Lett. **25,** 111–113 (2000).
7. R. Leitgeb, M. Wojtkowski, A. Kowalczyk, C. K. Hitzenberger, M. Sticker, and A. F. Fercher, "Spectral measurement of absorption by spectroscopic frequency-domain optical coherence tomography," Opt. Lett. **25,** 820–822 (2000).

8. S. A. Boppart, W. Drexler, U. Morgner, F. X. Kartner, and J. G. Fujimoto, "Ultrahigh resolution and spectroscopic optical coherence tomography imaging of cellular morphology and function," presented at the Inter-Institute Workshop on In Vivo Optical Imaging at the National Institutes of Health, Bethesda, Md., 16–17 September 1999.
9. B. Hermann, K. Bizheva, A. Unterhuber, B. Povazay, H. Sattmann, L. Schmetterer, A. F. Fercher, and W. Drexler, "Precision of extracting absorption profiles from weakly scattering media with spectroscopic time-domain optical coherence tomography," Opt. Express **12,** 1677–1688 (2004), http://www.opticsexpress.org.
10. C. Xu, J. Ye, D. L. Marks, and S. A. Boppart, "Near-infrared dyes as contrast-enhancing agents for spectroscopic optical coherence tomography," Opt. Lett. **29,** 1647–1649 (2004).
11. D. J. Faber, E. G. Mik, M. C. G. Aalders, and T. G. van Leeuwen, "Light absorption of (oxy-)hemoglobin assessed by spectroscopic optical coherence tomography," Opt. Lett. **28,** 1436–1438 (2003).
12. C. Yang, M. A. Choma, L. E. Lamb, J. D. Simon, and J. A. Izatt, "Protein-based molecular contrast optical coherence tomography with phytochrome as the contrast agent," Opt. Lett. **29,** 1396–1398 (2004).
13. L. Cohen, "Time–frequency distributions—a review," Proc. IEEE **77,** 941–981 (1989).
14. I. Daubechies, "The wavelet transform, time–frequency localization and signal analysis," IEEE Trans. Inf. Theory **36,** 961–1005 (1990).
15. R. Carmona, W. Hwang, and B. Torresani, *Practical Time–Frequency Analysis* (Academic, San Diego, Calif., 1998).
16. D. L. Jones and T. W. Parks, "A high resolution data-adaptive time-frequency representation," IEEE Trans. Acoust. Speech Signal Process. **38,** 2127–2135 (1990).
17. A. Papandreou-Suppappola, *Applications in Time–Frequency Signal Processing* (CRC Press, Boca Raton, Fla., 2002).
18. D. L. Marks, A. L. Oldenburg, J. J. Reynolds, and S. A. Boppart, "Digital algorithms for dispersion correction in optical coherence tomography for homogeneous and stratified media," Appl. Opt. **42,** 204–217 (2003).